RESEARCH ARTICLE

ADVANCED
INTELLIGENT
SYSTEMS
Open Access

www.advintellsyst.com

Smart Transfemoral Prosthetic Socket with Motorized Cable-Driven System

Linda Paternò,* Ahmed Zohaib Zaidi, Maria Grazia Polizzotto, Sofia Dalmiani, Djoeke Helsloot, Sybren Heikens, Emanuele Gruppioni, and Arianna Menciassi

Volume fluctuations in residual limbs can significantly affect the fit of prosthetic sockets, causing discomfort and instability when wearing a limb prosthesis. As a result, users must frequently visit prosthetic centers for socket adjustments or replacements, which is time-consuming and limiting. This study introduces a new transfemoral socket that incorporates a motorized cable-driven mechanism and a sensorized liner, allowing it to adapt to changes in residual limb volume based on interface pressures. Users can control the socket in both open- and closed-loop modes using a customized mobile application. The socket is able to withstand compressive mechanical loads of up to 900 N and demonstrates effective biomechanical coupling capabilities. A mathematical model guide the design of the system and is experimentally verified. To validate the system, an in vitro residual limb simulator with a hydraulic chamber is utilized, enabling volume adjustments of ±7.5%. In closed-loop mode, the smart socket effectively adjusts its volume to maintain interface pressure within the target range of 70–80 kPa. This innovative smart socket has the potential to enhance user satisfaction by allowing individuals with lower limb amputations to self-adjust their sockets as needed, ensuring a proper fit and safe interface pressures on tissues.

1. Introduction

Recent advancements in limb prostheses have led to innovative smart solutions, transforming traditional approaches and improving the quality of life for millions of people living with limb loss.[1] However, studies and surveys continue to report consistent dissatisfaction regarding the comfort and stability of limb prostheses, particularly among people with lower limb amputation.[2–5] Indeed, 57% of people with lower limb amputations report discomfort,[6] and 50% experience pain while using their prostheses.[7,8] This dissatisfaction is largely attributed to the inherent limitations of traditional prosthetic sockets.[1,3]

The socket serves as the physical human–machine interface between the user's body and the prosthetic device. It replicates the shape of the residual limb to ensure proper biomechanical coupling by gripping bony prominences and utilizing a suspension system. The suspension system typically relies on either the suction effect created by a unidirectional valve integrated into the socket or a pin-locking mechanism that secures the liner (i.e., a silicone sock worn between the residual limb and the socket) to the prosthetic attachment at distal base of the socket. However, as a rigid, passive structure, the socket cannot adapt to the volume changes of the residual limb over time, which can lead to discomfort, instability, and reduced prosthesis performance.

Following amputation, the volume of the residual limb undergoes a significant decrease, attributed to factors such as edema reabsorption and muscle atrophy,[9] but people with stabilized amputations (i.e., after 18 months from amputation) also experience volume fluctuations, including both increases and decreases. In the long term, these changes are often associated with weight gain and decreased levels of physical activity, but short-term volume changes also occur because of fluid movement in the body on the daily level. In a previous clinical study, the authors demonstrated a two-term decay exponential trend with a maximum volume change of +5.9% in transfemoral residual limb volumes after prosthesis removal and a volume change between −1.4% to +3.2% due to physical activity.[10]

The inability of traditional sockets to accommodate body volume fluctuations causes relative movements between the socket and residual limb, altered pressure distributions on tissues, and high shear stress on the skin. In transfemoral sockets, interface pressures can range from 40 to 150 kPa[11] and improper fitting results in pain, skin abrasions, and various dermatological issues. In more severe cases, volume changes

L. Paternò, A. Z. Zaidi, M. G. Polizzotto, S. Dalmiani, D. Helsloot, S. Heikens, A. Menciassi
Sant'Anna School of Advanced Studies
The BioRobotics Institute
Viale Rinaldo Piaggio, 34, 56025 Pontedera, PI, Italy
E-mail: linda.paterno@santannapisa.it

E. Gruppioni
Italian National Institute for Insurance against Workplace Accidents - INAIL Centro Protesi
Via Rabuina, 14, 40054 Vigorso, BO, Italy

**ADVANCED
SCIENCE NEWS**

www.advancedsciencenews.com

**ADVANCED
INTELLIGENT
SYSTEMS**

www.advintellsyst.com

can even make the prosthesis unwearable. Consequently, patients frequently need to visit the prosthetist either for socket adjustments or to obtain a new socket, which is both time-consuming and financially burdensome. Adjustable sockets integrating smart technologies could offer a solution. By modulating the socket volume based on pressure on the tissues, they could ensure a proper biomechanical coupling with the residual limb, providing a long-term solution that balances stability and comfort.

According to the literature, manually adjustable sockets have existed since 1960s and their quality has improved over the years.[12] Among current commercial solutions, RevoFit and RevoSurface by ClickMedical,[13] Varos by Ottobock,[14] ConnectTF by Ossur,[15] and Quatro by QuorumProsthetics[16] have movable parts that can be adjusted using cable systems, while Infinite Socket by LimInnovation[17] and Socket-less Socket by MartinBionics[18] use ratchet straps, and iFit Transfemoral system by iFIT Prosthetics[19] uses buckles to adjust the socket. Nevertheless, none of the existing solutions are capable of automatically adapting to volume changes in the residual limb or providing feedback to the user on proper fitting. As a result, patients often tighten the socket excessively to enhance perceived stability. Over-tightening and excessive pressure on tissues can lead to dermatological issues, restricted blood circulation, and further fluctuations in residual limb volume. Therefore, there remains a significant unmet need for prosthetic sockets that integrate smart technologies to ensure comfortable fitting at user's convenience.

Recently, both pneumatic and motor-driven sockets for lower limb prostheses have been proposed. Specifically, adjustable pneumatic sockets using an air pump connected to one,[20] two,[21] or three[4] soft chambers were developed and preliminary tested on either a single subject or an in vitro simulator. Nevertheless, pneumatic actuation for self-adjustable lower limb sockets can result in user-perceived instability and/or high-power consumption due to the compressibility of air and the significant cyclic forces acting at the socket interface. Hydraulic actuation can address these issues but leads to excessive weight and encumbrance of the final system. Another approach was proposed by Weathersby et al. who developed a smart transtibial socket with three movable panels and a cable-driven system that can be controlled by either a single motor[22] or three separate motors.[23] While this solution showed promising results, it does not allow for uniform socket adaptation to the residual limb, as only three panels of the total structure can be adjusted in the event of a volume change. Consequently, these designs are unable to accommodate volume increases and rely on applying high pressure at panel regions in the case of volume reductions, increasing the risk of high tissue stress. In the realm of motorized cable-driven mechanisms, more advanced solutions have been proposed for the active anchoring of exoskeletons, for instance, utilizing a corset design based on moving pulleys.[24] However, similar approaches have never been explored for improving the fit of limb sockets.

In this context, the present article introduces a new smart prosthetic socket system for transfemoral amputees (**Figure 1**). With respect to previous designs with movable panels, this system offers enhanced adaptability to the residual limb, promoting a more even pressure distribution and reducing the risk of dermatological issues, thanks to a custom-designed prosthetic attachment with two rotational joints and a cable-driven pulley system located in the anterior and posterior sides of the socket structure. The custom-designed prosthetic attachment allows for the simultaneous and symmetric adjustment of the medial and lateral parts of the socket, while the cable-driven pulley system ensures the transmission of a more uniform force along the length of the structure. The socket system integrates a sensorized prosthetic liner and a wearable control unit, which includes a motor connected to the cable-driven mechanism and an electronic circuit for control. The socket volume can be controlled in both open- and closed-loop modalities via a customized mobile application. Such a system has the potential to minimize common issues such as excessive tissue compression, discomfort, and skin abrasions by enabling users to monitor socket-residual limb pressures. Additionally, the socket can be activated in the closed-loop modality to automatically adjust to the residual limb each time the prosthesis is worn, or discomfort is felt, exploiting user-specific pressure thresholds. This approach aims to improve the fit, potentially reducing the need for frequent prosthetist visits and socket replacements. An in vitro residual limb simulator with variable volume was developed to assess the performance of the proposed solution.

The following sections offer a detailed explanation of the design and development of the smart socket system components, along with the results obtained from in vitro validation. These results demonstrate the effectiveness of the final device and are discussed in terms of the potential of smart socket solutions to significantly improve the quality of life for individuals living with limb amputations.

2. Results and Discussion

2.1. System Overview of the Smart Prosthetic Socket System

The design of the smart prosthetic socket system, illustrated in Figure 1, includes an adjustable socket system, a wearable control unit, and a mobile app. The adjustable socket system consists of three layers: a sensorized liner, a flexible socket, and a rigid socket with a cable-driven mechanism. These three layers are connected to a custom prosthetic attachment at the distal base, allowing integration with commercial prosthetic knees. Four commercial sensors are embedded in the prosthetic liner and positioned in contact with the skin to monitor the average pressure applied to the residual limb tissues. The system is controlled by the user through a mobile application, which communicates with the control unit via bluetooth low energy standard. The control unit can adjust the cable length through a DC motor and a reduction gear system to optimize the socket fit. Specifically, the system supports an open-loop control of the motorized cable-driven mechanism to enable users to adjust the socket volume while monitoring interface pressure, thus preventing over-tightening and excessive pressure on the tissues. Additionally, users can activate an automatic adjustment of the system in closed-loop control based on preset, user-specific pressure thresholds, ensuring optimal fitting each time they wear the prosthesis or deem it necessary.
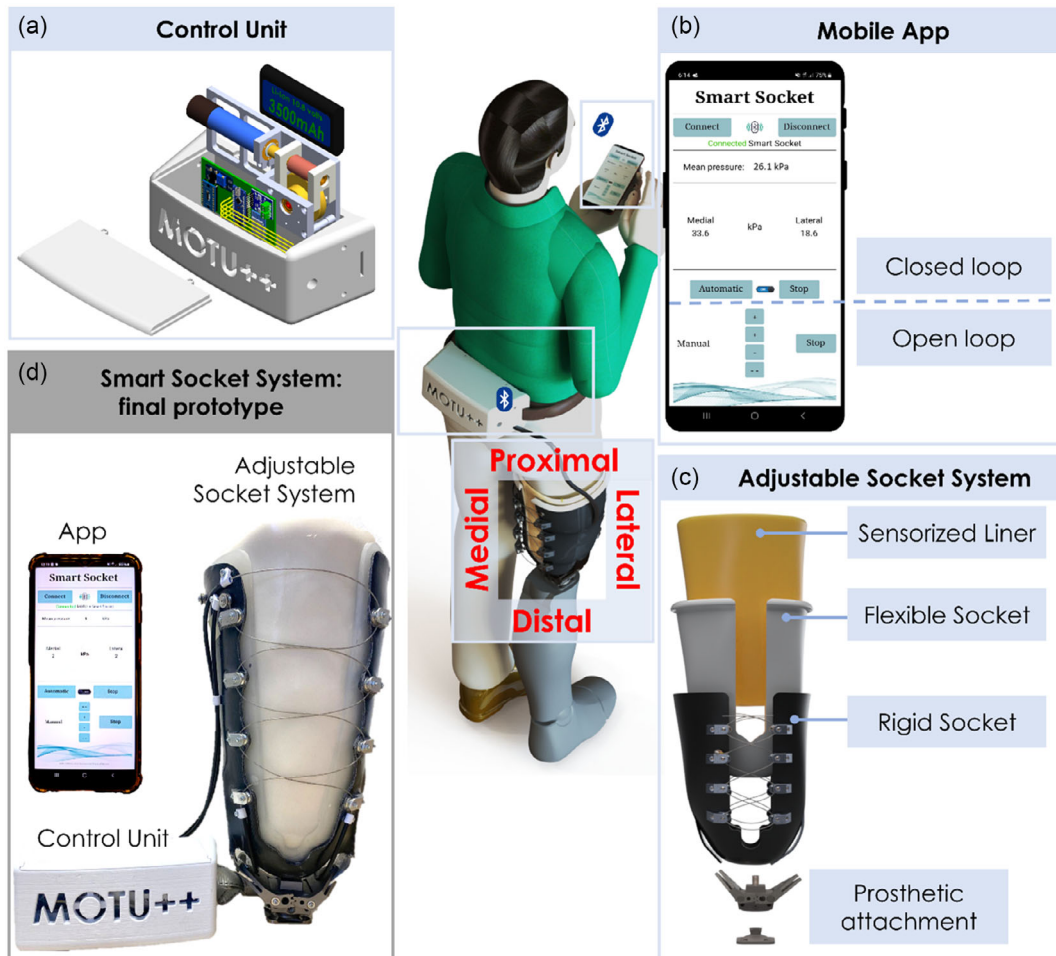
Figure 1. a–c) Design overview and d) final prototype of the smart socket system. The proposed solution includes: (a) a wearable control unit composed of a DC motor coupled with a reduction gear system, an electronic circuit, and a battery; (b) a mobile app that enables the socket to adapt to the residual limb in both open- and closed-loop modes, communicating with the control unit via Bluetooth; (c) an adjustable socket system consisting of a sensorized prosthetic liner, a flexible socket, a rigid socket with a cable-driven mechanism on both the anterior and posterior sides, and an ad-hoc prosthetic attachment.

2.2. Adjustable Socket System

2.2.1. Custom Prosthetic Attachment

The design of the adjustable socket system began with the custom prosthetic attachment. As shown in **Figure 2**a, traditional prosthetic attachments feature an upper part with fixed flanges integrated into the socket structure and a bottom pyramid adapter secured to the prosthetic knee with four screws. The pyramid adapter is locked onto the upper part using four set screws, allowing for proper alignment between the prosthetic knee and the socket. To achieve a structure capable of uniformly adapting to the volume changes of the residual limb without relying on a design with movable panels as done in previous solutions,[22,23] it becomes necessary to develop a new attachment. This attachment must allow for the symmetric movement of the various parts into which the socket is divided, enabling the adaptation of the entire structure to the residual limb. This ensures that no areas of the residual limb experience significantly higher pressure than others, enabling even compression of the entire residual limb and the effective distribution of applied forces required for biomechanical coupling.

Concept selection was performed using the Harris profile, a design tool that visually compares different concepts based on multiple weighted criteria, allowing for an easy evaluation of strengths and weaknesses of each concept. The selected performance criteria, in decreasing order of importance, were as follows: weight, considering all components; complexity, determined by the number and type of components and their general layout; encumbrance, based on the arrangement of components; adaptation range to the residual limb, estimated by the type of joints and range of movement; pressure distribution on tissues, assessed by the type of joints and their ability to apply uniform pressure along the socket structure, considering that the volume changes of the residual limb usually occur relatively uniformly along the limb; and strength, based on the number of joints. It should be noted that in all the designs analyzed, a single cable wrapping around the entire socket
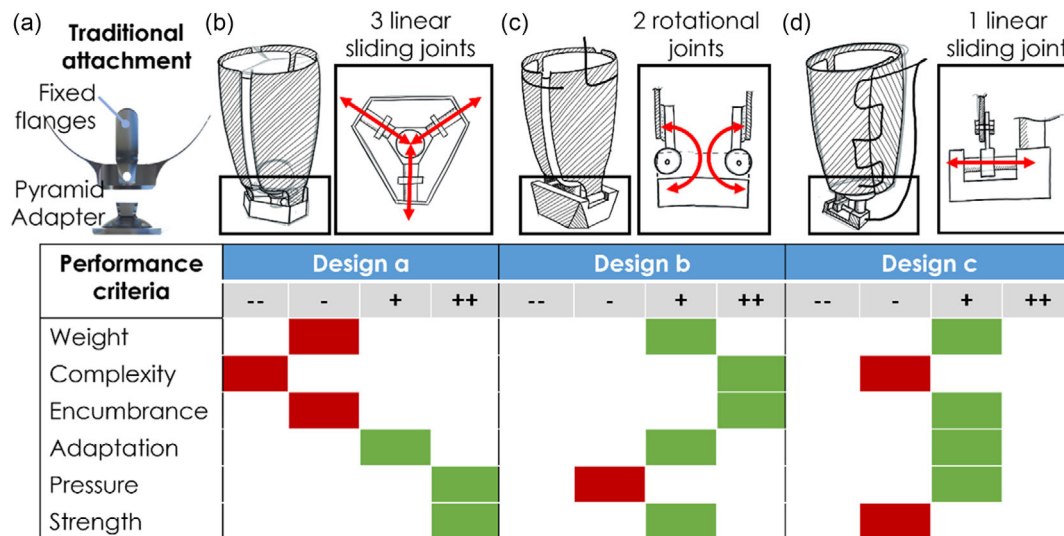
2400995 (3 of 16)

**ADVANCED
SCIENCE NEWS**

www.advancedsciencenews.com

**ADVANCED
INTELLIGENT
SYSTEMS**
Open Access

www.advintellsyst.com

Performance criteria	Design a				Design b				Design c			
	--	-	+	++	--	-	+	++	--	-	+	++
Weight		■					■				■	
Complexity	■							■	■			
Encumbrance		■						■			■	
Adaptation			■			■					■	
Pressure				■	■						■	
Strength				■			■		■			

Figure 2. a) Traditional prosthetic attachment featuring fixed flanges integrated into the socket structure and a pyramid adapter fixed at the prosthetic knee. b–d) The Harris profile tool was used for the selection of the initial concept of the custom prosthetic attachment of the adjustable socket system. The three analyzed designs featured: (b) three linear sliding joints; (c) two rotational joints; (d) a single linear sliding joint. ++ : excellent + : good; - : poor; -- : very poor.

structure and passive attachment joints were considered. This configuration requires only one motor and allows the socket structure to adapt when the cable is tightened or loosened.

The first analyzed design utilized three linear sliding joints (Figure 2b), which enhanced the strength of the mechanism and ensured more uniform pressure distribution and symmetric adaptation along the length structure. However, the weight, complexity, and overall size of this design were likely too high for a lower limb prosthesis. Additionally, the volume compensation capabilities were limited due to space constraints, which affected the total possible displacement of the linear joints. The second concept used two rotational joints (Figure 2c), making it a proven and straightforward design. Reducing the number of joints and using rotational instead of linear joints decreased the weight, complexity, and overall size of the attachment. The adaptation in this design was less symmetrical along the length structure, and the pressure distribution was less uniform compared to the first design, but with a properly cable-driven mechanism in the socket structure, these factors could be improved. The third design (Figure 2d) was based on a single linear sliding joint. This had the potential to reduce the system weight, and the linear motion ensured a uniform pressure distribution on the residual limb. However, careful consideration was required in the bearing design of the joint to prevent jamming and maintain structural integrity, which added complexity and bulk to the final design.

Based on the aforementioned considerations, the second design with two rotational joints was selected as a good balance between simplicity, encumbrance, and performance. While uniform pressure distribution remains a key priority for this work, other factors, such as size and weight, are critical to ensuring the system's usability and overall feasibility. Although the other designs may provide more uniform pressure distribution, this can be also improved through additional components, such as a specific coupling between the two rotational joints

to enhance symmetry between the lateral and medial movable parts of the socket system by constraining them to a single degree of freedom. Furthermore, an anterior-posterior cable-driven pulley mechanism can ensure more even load distribution along the socket length, as demonstrated in the following sections. These features address the limitations of the two rotational joint configurations while maintaining its practical advantages of reduced size, weight, and complexity, resulting in a functional and feasible solution for long-term use.

Optimization studies were performed in SolidWorks to generate new design iterations and define the final prosthetic attachment, shown in **Figure 3**.

The final prosthetic attachment features two movable flanges capable of rotating about the sagittal axis relative to a central base.
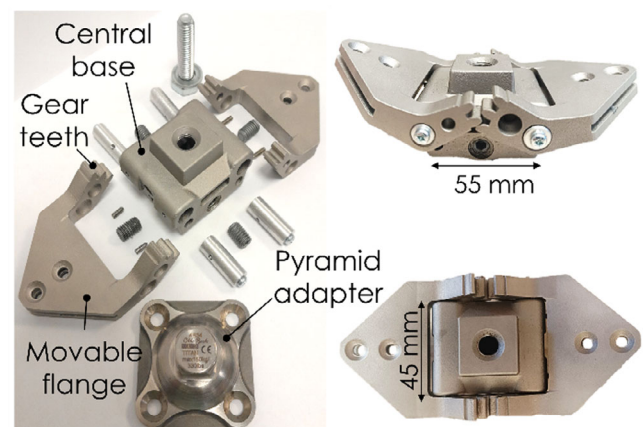

Figure 3. Ad hoc prosthetic attachment designed for the proposed adjustable socket system. The attachment features two movable flanges with gear teeth that can rotate relative to the central base. The central base can be coupled at the bottom with a commercial pyramid adapter, allowing it to be mounted on a prosthetic knee.

**ADVANCED
SCIENCE NEWS**

www.advancedsciencenews.com

**ADVANCED
INTELLIGENT
SYSTEMS**
Open Access

www.advintellsyst.com

The bottom part of the central base replicates commercial solutions, allowing it to be mounted on a traditional commercial male pyramid adapter (here the Ottobock 4R54) to connect the socket to a prosthetic knee joint. The flanges enable easy mechanical coupling based on screw mechanisms with two metal bars to be integrated into the rigid socket at the medial and lateral sides. Two dissimilar cut-outs in the flanges keep the center of mass of the entire mechanism at the central axis. A spur geared coupling between the two flanges constrains the degrees of freedom to one for improving symmetry. To design the gear teeth of the flanges, Lewis's formula was used to calculate the bending stress, while Hertz's formula was applied to determine the contact pressure on the teeth. These values were then used to calculate the Von Mises stresses, and the final design was analyzed through finite element method simulations (see "Custom Prosthetic Attachment: Design and Simulations"). Starting from a configuration at 45° relative to the base, the two flanges can rotate up to 20° in both directions before losing contact, which provides more than sufficient range for the operational requirements of the application under analysis. Since fabricating the prosthetic attachment in Ti–6Al4V requires specialized machinery, an initial prototype was produced using direct metal laser sintering technology with 316 stainless steel. In the future, Ti–6Al4V will be used to achieve greater strength and a reduction in weight (i.e., 395 g instead of 710 g for the current prosthetic attachment prototype).

2.2.2. Adjustable Socket

The adjustable socket structure consists of a flexible socket, thermoformed from a 12 mm-thick layer of Thermoflex plastic, positioned between the rigid socket and the liner (**Figure 4**). The flexible socket provides a low-friction interface on which the rigid socket, equipped with the adjustable cable-driven mechanism, can slide smoothly. Specifically, the liner, flexible socket and rigid socket are secured together solely at the distal end, thanks to the mechanical pin of the liner that passes
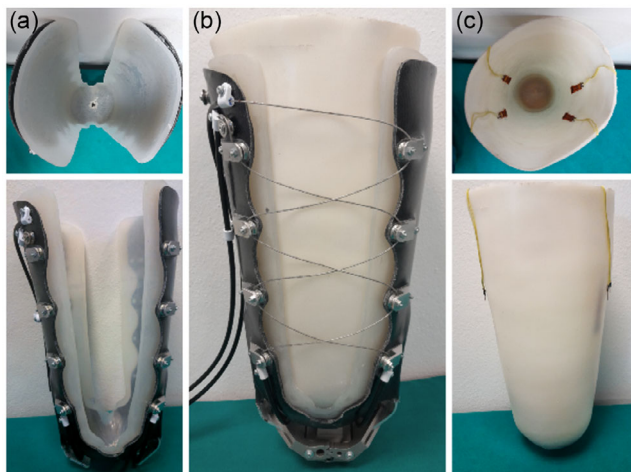
through the flexible and rigid sockets and attaches to the base of the prosthetic attachment. Both the rigid and flexible sockets feature a U-shaped profile, like traditional sockets with openings in the anterior and posterior regions. This design applies a mediolateral grip on the residual limb required to properly align the amputated femur with the prosthesis axis.[25] The rigid socket was made of carbon fiber-reinforced resin using lamination technique, providing high mechanical strength, durability, and a lightweight design. As anticipated, two metal bars (3 mm thick, 4 cm × 15 cm, aluminum) were integrated into the rigid socket at the medial and lateral sides to simplify the integration with the movable flanges of the custom prosthetic attachment. Specifically, the metal bars were directly bonded with carbon fiber-reinforced resin during lamination to ensure proper integration of the two materials. Indeed, conventional screw joining methods often lead to high-stress concentrations and premature failure in the resin structure. Multiple samples with different designs of the metal bars were tested to analyze the strength of the bonding interface, since the stiffness difference between the two materials can also contribute to potential structural failures (see "Rigid Socket: Design Selection of the Metal Bars", Figure 10). Contrary to expectations, the design with the highest strength turned out to be the plain design (Figure 10), which was then used in the final prototype.

The rigid socket features a cable-driven system based on a pulley mechanism at both the anterior and posterior sides, enabling a high tightening force between the lateral and medial parts of the socket with a lower cable tension force. Specifically, 16 pulleys (12 mm diameter, stainless steel, V-groove type) are fixed through metallic brackets on the external surface of the rigid socket. A Bowden cable passes through the pulleys and its length and tension can be regulated by the control unit to compress and release the residual limb.

At high contractions, localized stresses can arise where the two halves of the socket converge. To further enhance its mechanical performance, a stress-relief mechanism has been designed in the central part to minimize bending stresses during adjustments. Additionally, the incorporation of rotational joints in the prosthetic attachment, the spur-geared coupling between the two movable parts of the prosthetic attachment, and the pulley system ensure symmetrical adjustments. This design enables an even distribution of forces across the entire socket structure, rather than concentrating them at the attachment point. Finally, the socket is constructed from carbon fiber-reinforced resin, a material renowned for its high tensile strength and excellent fatigue and bending resistance.

2.2.3. Sensorized Liner

The adjustable socket system interfaces with skin through a prosthetic liner made of 617H43 Silicone Gel (Ottobock), providing a soft and high-friction surface against residual tissues (Figure 4c). The high friction coefficient of silicone gel and the large contact area with the skin make it possible to generate a high frictional force with less pressure, while guaranteeing a safe and comfortable interface. The prosthetic liner can be secured to the custom prosthetic attachment at the distal end of the socket using a pin-locking mechanism.

Figure 4. a) Outer rigid (black) and inner flexible (white) sockets; b) final adjustable socket system with cable-driven mechanism; c) silicone prosthetic liner with four embedded FSR sensors.

**ADVANCED
SCIENCE NEWS**

www.advancedsciencenews.com

**ADVANCED
INTELLIGENT
SYSTEMS**

www.advintellsyst.com

In the liner, four commercial force-sensing resistor (FSR) sensors (FlexiForce A201 sensor, Tekscan) are embedded to monitor pressure on tissues at the lateral and medial sides. These sensors were selected due to their simple, low-cost design, making them a practical solution for system validation.

The mean interface pressure (MIF) between the residual limb and the socket during double support standing in transfemoral amputees was used as the target range for the closed-loop control. Indeed, the proposed solution is not designed for continuous adaptation during daily activities but rather as a system that can be activated by the user when the prosthesis is worn or whenever needed. The mean pressure during double support standing typically falls within the range of 70–80 kPa.[26–28] Thus, the sensors were calibrated up to 140 kPa to ensure comprehensive coverage of the pressure values under analysis. The average hysteresis of the four FSR sensors was found equal to 3.9 ± 1.2 kPa with 33.3 ± 19.3 kPa linearity (see "Suspension Performance of the Adjustable Socket System"). While these performances are sufficient for validating the feasibility of the proposed system, alternative sensor technologies will be explored for long-term consistency and reliability.[29,30]

Considering the socket design, two FSR sensors were positioned on the medial side and two on the lateral side of the liner.

2.3. Transfemoral Residual Limb Simulator with Variable Volume

Short-term volume fluctuations of residual limbs are primarily caused by the movement of body fluids, which can be influenced by a complex combination of factors such as physiological and biometric characteristics, age, lifestyle, residual limb condition after amputation, and pressure applied by the user-specific socket. This intricate interplay can result in significant variability, making it challenging to test the proposed solution effectively.

Recent advancements in soft robotics have led to the development of numerous physical simulators, providing a powerful alternative to in vivo testing.[31,32] By simulating human body parts with materials that mimic the properties of natural tissues and replicate natural motion, these systems can offer advanced platforms to validate new devices in a more controlled and efficient manner, particularly in the early stages of technological

solutions development. Thus, an in vitro high-fidelity physical simulator of a transfemoral residual limb was developed to evaluate the performance of the proposed solution (**Figure 5**).

The simulator houses a hydraulic chamber that allows for effectively replicating volume fluctuations due to body fluid movements observed in transfemoral residual limbs. For the skeletal structure of the simulator, an anatomical functional model of the hip joint (model NS 51, SOMSO-PLAST) was employed, while silicone materials were utilized to build the muscles, fat, and skin, closely resembling the mechanical properties of lower residual limb tissues (see "Mechanical Performance of the Adjustable Socket System" for additional details).[33] A 3D printed attachment was created to fix the simulator at the proximal end starting from the 3D scan of the hip anatomical model. The hydraulic chamber was connected to two motorized syringe pumps (model NE-1010, New Era Pump Systems, Inc., USA), allowing for controlled volume fluctuations of the simulator through water injection.

The simulator volume was measured at different inlet water volumes with 100 cm³ intervals, using a 3D scanner (model GO! SCAN50, Creaform Inc.). The procedure was repeated three times to ensure accuracy and consistency in the results. The initial volume (V_0) of the simulator, when the fluidic chamber was empty, was determined to be 3836.5 ± 19.1 cm³. It was increased up to 4123.4 ± 18.7 cm³ when the fluidic chamber was filled with 300 cm³ of water (i.e., ≈7.5% volume increment). This volume range ensures that the simulator can replicate the total, and even greater, short-term volume fluctuation range measured in the previous clinical study involving 24 people with transfemoral amputation.[10] Indeed, the maximum percentage change observed in the clinical study was +5.9%, which required the injection of ≈ 230 cm³ of water, as indicated by the black dashed line in Figure 5. Obviously, the simulator can also be used to simulate volume reductions if the initial volume is considered as the volume with the injected water.

2.4. Characterization of the Adjustable Socket System

The proposed design of the socket system can be approximated as a truncated cone with a hemispherical shape at the distal base, as shown in **Figure 6**a. Due to the socket design, the volume of
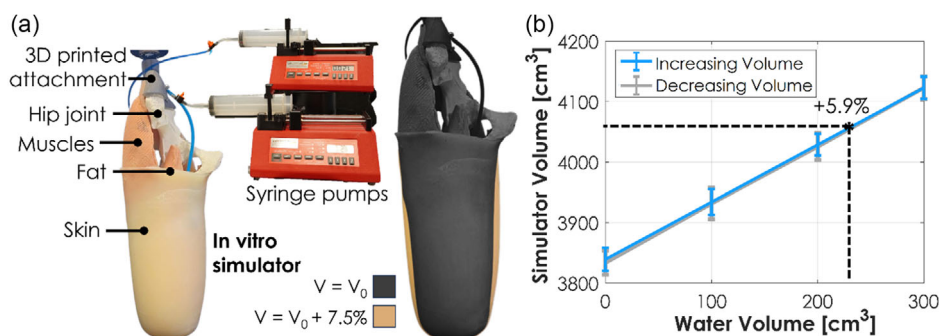

Figure 5. a) In vitro simulator of a transfemoral residual limb. The simulator can mimic the volume fluctuation of residual limbs thanks to a hydraulic chamber connected to two motorized syringe pumps. b) The volume of the simulator was measured using a 3D scanner at different inlet water volumes injected into its hydraulic chamber. The volume was increased (blue values) and decreased (gray values) three times up to 300 cm³ of water (i.e., +7.5%) in 100 cm³ steps.

ADVANCED
SCIENCE NEWS
www.advancedsciencenews.com

ADVANCED
INTELLIGENT
SYSTEMS
Open Access
www.advintellsyst.com

the hemispherical part (V_h) can be considered as a constant, and the volume changes of the structure can be attributed solely to the volume changes of the conical part (V_c). Therefore, it can be stated that

$$V_{socket} = V_c + V_h = \frac{1}{3}\pi h(r_1^2 + r_1 r_2 + r_2^2) + \frac{2}{3}\pi r_1^3 \qquad (1)$$

$$\Delta V_{socket} = \Delta V_c = \frac{V_{cf} - V_{ci}}{V_{ci}} \qquad (2)$$

The pulleys of the cable-driven mechanism are used to distribute the applied force around the residual limb, ensuring a more symmetric adaptation (Figure 6b). Specifically, each pulley aids in distributing the cable tension across the contact surface of the socket and, for simplicity, we can approximate that the cable tension is equally distributed by each pulley. The cable tension force (T), the transmitted force around tissues (F), and the interface pressure (P) can be correlated as follows (Figure 6c):

$$P = \frac{F}{A} = \frac{N T \varphi}{\varphi (r_1 + r_2) l} = \frac{N T}{(r_1 + r_2) l} \qquad (3)$$

where A is the lateral area of the conical part of the socket, and φ refers to the angle of contact between the socket and the residual limb (see Figure 6c). $N = 16$ represents the total number of pulleys, as the force is equally transmitted along the entire cable. Using this formula, it is possible to calculate the tension force required to achieve an interface pressure of 80 kPa when the socket structure is fully in contact with the residual limb. In this condition, the proximal radius, r_2, can be considered equal to the radius of the simulator plus the thickness of the socket system, resulting in a value of 8.6 cm. Thus, a tension force of around 191 N is expected.

Furthermore, considering the symmetry at the anterior and posterior sides of the cable-driven mechanism, the length of the cable on each side of the socket can be defined as (Figure 6b):

$$L = w + \frac{w}{\cos \alpha}(N - 2) + L_1 \qquad (4)$$

where $N = 8$ is the number of pulleys on each side of the socket, and L_1 is constant due to the rigid cable guides in the socket structure. Considering the value of r_2 in the resting expanded

state of the system equal to 9.2 cm, and approximating $\Delta w \approx \frac{\Delta C_2}{2}$, where ΔC_2 is the circumference variation at the proximal area, a shortening ΔL of $\approx$14.6 cm is expected on each side to achieve the desired configuration in which the socket is in contact with residual limb simulator (i.e., $r_2 = 8.6$ cm). However, due to the complexity of the system, experimental tests were conducted to validate the above assumptions and precisely characterized the proposed system.

For the tests, the prosthetic liner of the socket system was rolled onto the simulator, which was then positioned within the socket system. The liner was fixed to the prosthetic attachment that was subsequently fixed to the base of an Instron Testing Machine. The cable of the adjustable mechanism was pulled from both ends at the same time, starting from the socket system's resting configuration ($L_0 = 270$ cm, $r_2 = 9.2$ cm). Tests were conducted at different simulator volumes: $V = V_0$ pulling the cable of 24 cm, $V = V_0 + 100$ cm^3 pulling the cable of 20 cm, $V = V_0 + 200$ cm^3 pulling the cable of 16 cm, $V = V_0 + 300$ cm^3 pulling the cable of 12 cm. For each volume condition, seven tests were performed, while measuring the pulling force with the Instron Testing Machine load cell and the interface pressure with the FSR sensors embedded in the prosthetic liner of the socket system. Results are reported in **Figure 7**.

Base on obtained results, the actuation system in the control unit should provide a force in the range of 0–250 N. This information was considered for the final design of the control unit. Additionally, a cable shortening of $\approx$14.5, 14, 9, and 6 cm is required to reach the target pressure range of 70–80 kPa at simulator volumes of $V = V_0$, $V = V_0 + 100$ cm^3, $V = V_0 + 200$ cm^3, $V = V_0 + 300$ cm^3, respectively, as indicated by the black dashed lines in Figure 7 which indicate the 75 kPa value. As expected from theoretical evaluation ($T = 191$ N) a force of about 200 N is required to apply an interface pressure of 80 kPa at $V = V_0$.

Finally, suspension tests were conducted using an Instron Testing Machine to evaluate the effectiveness of the proposed solution in achieving proper biomechanical coupling with the residual limb, following the experimental protocol outlined in the state of the art.[34–36] The results demonstrated that the relative displacement between a mock residual limb (pulled by the Instron) and the socket (fixed at the base) was minimal. Specifically, the displacement measured 0.26 ± 0.01, 0.11 ± 0.01, and 0.11 ± 0.01 mm for 12, 14.5, and 17 cm cable length
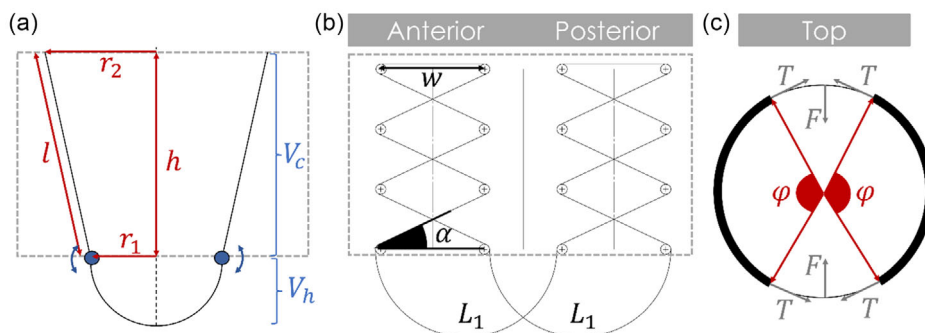

Figure 6. Design parameters used in the mathematical evaluation of the tension and cable length change required in the operating range of the smart socket system (with r_1 and l considered constant, at 6.5 and 25 cm, respectively). a) The structure of the adjustable rigid socket is approximated as a truncated cone with a hemispherical shape at the distal end. b) A cable-driven mechanism is integrated into the anterior and posterior sides to facilitate a more symmetric adjustable structure along the length of the structure ($\alpha = 28°$). c) Schematic representation of the residual limb compression model.
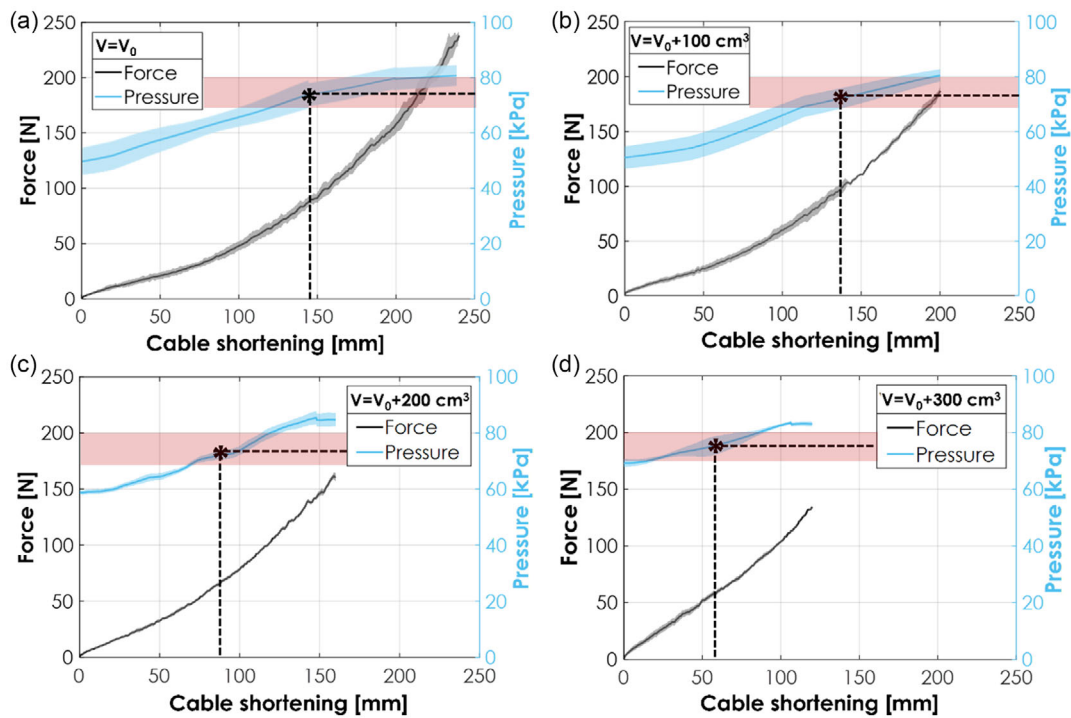
Figure 7. The force required to pull the cable of the adjustable socket system, along with the interface pressure, was measured a) at the initial volume and after volume increases of b) 100 cm³, c) 200 cm³, and d) 300 cm³ in the in-vitro simulator. These measurements were taken while shortening the cable by 24, 20, 16, and 12 cm, respectively. For each condition, 7 tests were carried out. Red areas indicate the 70–80 kPa pressure range.

shortening, respectively, at a tension load of 100 N on the mock residual limb. At a tension load of 650 N, the displacement was 1.68 ± 0.06, 1.36 ± 0.01, and 1.14 ± 0.01 mm for 12, 14.5, and 17 cm cable length shortening, respectively. These results indicate excellent suspension performance. Additionally, the socket was able to withstand compression mechanical loads of up to 900 N. See "Suspension Performance of the Adjustable Socket System" for additional details.

2.5. Control Unit and Mobile App

The control unit of the smart socket system includes a Faulhaber DC motor with a maximum torque of 0.7 Nm, which is coupled with a planetary gearbox with a reduction ratio of 43:1. The output shaft of the gearbox is connected to a worm gear system, which consists of a single-thread worm and a worm wheel with a cylindrical protrusion, around which the cable is wound. See "Sensorized Liner: FSR Sensors Calibration" for additional details.

The control unit also includes a printed circuit board (PCB) incorporating an Arduino Nano microcontroller. It is powered by a 10.8 V 3500 mAh Li-Ion rechargeable battery. The backup time of the battery was calculated to be $\approx$4 h 20 min based on the average current consumption of the motor at high speed. However, the system is supposed to be activated only a few times per day to accommodate changes in residual limb volume, thereby extending battery life (up to a week considering $\approx$8 activations per day). The control unit can be placed inside a wearable case with a textile belt.

The control unit can be commanded by the user using a mobile application (Figure 1) that was designed in the MIT App inventor environment. From the top of the screen (Figure 1b), the app interface features Bluetooth connection options and status. These are followed by a real-time display of the mean of the four FSR pressure values and the mean values for the medial and lateral side sensors. The system uses a finite-state machine algorithm to act on different functions in the manual and automatic modes. Whenever the system receives a command, a switch state is defined to check a series of conditions based on MIF. If the automatic mode is activated, a threshold-based controller starts to continuously monitor the MIF along with an exit command. If MIF < 50 kPa, the motor actuates to tighten the socket; if 50 kPa < MIF < 70 kPa, the motor runs to tighten the socket but at slower speed; if 70 kPa < MIF < 80 kPa, the motor is stopped to keep the socket volume constant; if 80 kPa < MIF < 100 kPa, the motor slowly loosens the socket and if MIF > 100 kPa, the motor activates to loosen the socket at a faster speed. As soon as it receives the exit command, it stops the motor and exit automatic mode. In the bottom part of the app interface, there is the manual mode tab that features four buttons for the open-loop control of the system. The user can press the following buttons "++", "+", "-", and "--", which correspond to predefined switch cases. By clicking on "++" and "+" the motor runs in the clockwise direction at two different speeds to release the socket, while clicking on "--" and "-" the motor runs in the counterclockwise direction to tighten the socket at two different speeds. The "Stop" button can be used to end any of the manual options.

The system employs a threshold control strategy to maintain an interface pressure during double-stance standing within a preset range of 70–80 kPa. However, in the future, the prosthetist will be able to easily adjust the range to meet user-specific needs.

Since volume changes in the residual limb occur gradually throughout the day, and the interface pressure profile varies significantly depending on the user's activities,[11] the smart socket system can be activated each time the prosthesis is worn or as needed, avoiding continuous adaptation. This approach also extends battery life and reduces motor wear. Unlike current commercial sockets, which have a fixed volume, our design introduces flexibility, aiding users in achieving a proper socket fit whenever required. In the future, a more advanced control strategy could be explored, potentially incorporating motion task detection algorithms for continuous operation. This would require a series of clinical trials to develop a pressure distribution pattern aligned with the entire gait cycle and other physical activities, rather than maintaining a static pressure range.

2.6. In Vitro Validation

The final system on a manikin is shown in **Figure 8**. The total weight of the device, including the adjustable socket system with the prosthetic attachment and the sensorized liner, and the control unit (comprising the DC motor coupled with the reduction gear system, the electronic circuit, and the battery), is 3.15 kg. However, the control unit (weighing 1.65 kg) can be positioned in a wearable case designed to be worn with a textile belt, similar to a fanny pack. In this way, the socket's weight amounts to 1.50 kg, aligning with that of currently used systems, which typically weigh ≈1.5 kg when accounting for prosthetic silicone liners.

Figure 8. Final prototype on a manikin, showcasing the footprint of the proposed system, including the wearable control unit, and the adjustable socket system.

To validate the proposed system, the in vitro simulator was employed to replicate changes in residual limb volume and assess the effective adaptation of the socket system. Specifically, the simulator at its initial volume V_0 was positioned within the socket system in its resting configuration (Step 0, **Figure 9**). In this state, the cable length of the socket system was 270 cm, and the MIF was recorded to be 61.9 ± 1.6 kPa, below the target range of 70–80 kPa. Consequently, when the automatic mode was activated, the socket system contracted by shortening the cable of 14.3 ± 0.9 cm, until the pressure reached the desired range (interface pressure equal to 75.8 ± 1.6 kPa) (Step 1, Figure 9). Next, the automatic mode was deactivated, and the simulator volume was increased by injecting 230 cm^3 of water (Step 2, Figure 9), corresponding to a volume change of ≈+5.9%, which reflects the maximum volume change observed in the previous clinical study.[10] This increase led to a rise in interface pressure beyond the target range (interface pressure equal to 88.0 ± 2.9 kPa). Once the automatic mode was reactivated, the socket system expanded by releasing the cable of 9.8 ± 1.0 cm, until the pressure returned to the desired range (interface pressure equal to 73.4 ± 1.4 kPa) (Step 3, Figure 9). This test was repeated six times and the repeatability of the results over multiple trials suggests that the system is capable of consistently maintaining a proper fit, minimizing the risks of discomfort and excessive tissue compression associated with traditional sockets. Additionally, these results indicate that the design maintains a high degree of symmetry during adjustments, although absolute symmetry is unattainable due to the irregular shape of patients' residual limbs. As depicted in Figure 9, in the resting state (Step 0), the interface pressure between the medial and lateral sides differs by 12.2 kPa, a difference mainly due to the socket shape defined by the prosthetist. After activating the automatic mode (Step 1), this difference was measured at 13.3 kPa, suggesting that the two halves of the socket have contracted in a relatively symmetric manner. Subsequent to the volume increase of the simulator (Step 2), the symmetry was impacted; indeed, this adjustment caused the pressure difference to increase to 28 kPa, likely due to an asymmetric expansion of the simulator. Following the expansion of the socket triggered by reactivating the automatic mode (Step 3), the results showed improvement with the pressure difference between the medial and lateral sides decreasing to 10.5 kPa. This decrease is likely due to the redistribution of water within the simulator, potentially mimicking similar changes with the bodily fluids in a residual limb.

A demonstration of the in vitro validation of the proposed smart socket system is also shown in Video S1, Supporting Information.

3. Conclusion

The smart prosthetic socket system presented in this study represents a significant advancement in addressing the critical challenge of compensating volume fluctuations in residual limbs over time. Unlike commercial sockets, the proposed system can adapt to changes in residual limb volume offering consistent and personalized adjustments by integrating both closed-loop and open-loop control modalities through a mobile application. Additionally, the system provides real-time feedback to users on
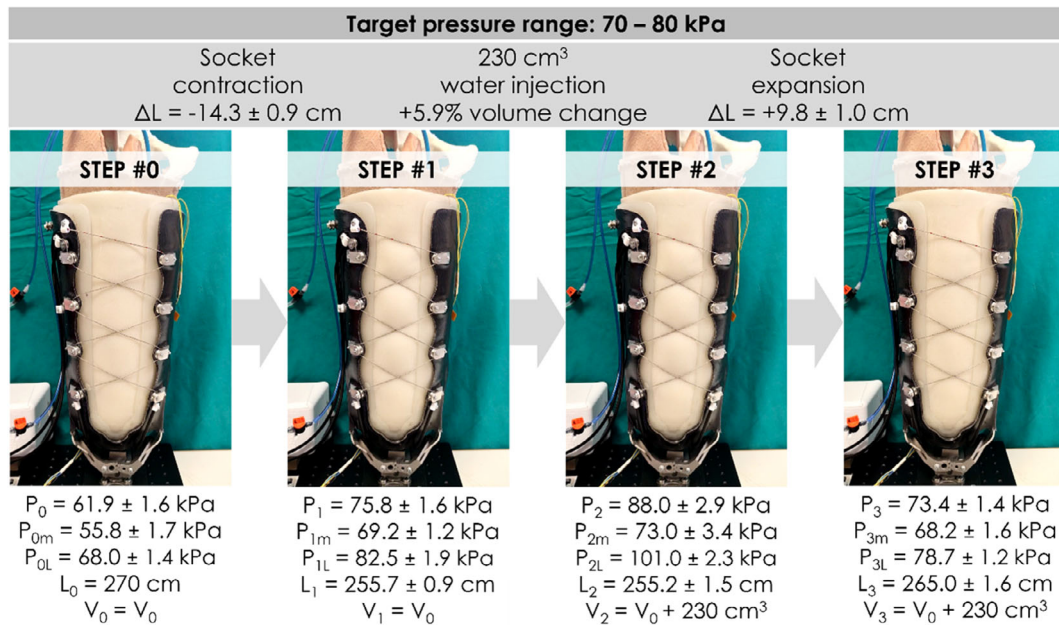
Figure 9. The in vitro simulator was used to replicate residual limb volume changes and assess the system effectiveness. After increasing the simulator volume by +5.9%, the socket system automatically adjusted to restore pressure within the target range. This process was repeated six times, monitoring interface pressure using sensors and cable length using the control unit. P_m and P_L represent the lateral and medial pressure, respectively.

the pressure applied to tissues. This approach holds great potential for preventing common issues seen with manually adjustable solutions, such as over-tightening, which can lead to discomfort, restricted blood circulation, and further volume changes. The proposed cable-driven mechanism incorporates pulleys to evenly distribute the cable tension, regulated by the DC motor in the control unit. This ensures more uniform adaptation across the entire socket structure, overcoming the uneven adjustments seen in previous designs,[22,23] that relied on only a few movable panels.

In vitro validation of the system demonstrated its ability to maintain interface pressure within the desired range under varying residual limb volumes. These promising results underline the potential of this system to significantly enhance user comfort and long-term socket performance.

The study presented in our article has some limitations. While the FSR sensors used in our smart socket provided a practical, low-cost solution for feasibility testing, they are limited by long-term stability, particularly under prolonged use and dynamic loading. To address these issues, future work will focus on developing and integrating customized sensor technologies tailored to the unique demands of the application.

Previous efforts to develop sensors for measuring pressure within prosthetic sockets have explored a variety of solutions, including piezoelectric,[37] capacitive,[38] or optical[39,40] sensors, each with specific advantages and drawbacks.[41–44] Piezoelectric sensors are highly sensitive to dynamic pressure changes and offer a good high-frequency response but are expensive, rigid, and unsuitable for flexible systems or static pressure measurements. Capacitive sensors provide high accuracy but are sensitive to environmental factors like humidity and suffer from nonnegligible crosstalk, requiring complex shielding and circuitry, which increase cost and integration challenges. Optical

sensors, such as fiber Bragg gratings, offer several benefits, including high sensitivity. However, they also require bulky detection systems, and they are highly susceptible to damage.

Future iterations of this work will prioritize the development of robust, soft sensing technologies, seeking the best trade-off for the application under analysis while aiming to minimize the described limitations. These advancements will focus on improving sensor durability, maintaining sensitivity over time, and ensuring reliable pressure measurements under static and dynamic conditions using soft materials, thus enhancing the overall performance and comfort of the prosthetic socket.

Defining the optimal fit of a prosthetic socket is inherently challenging, as each socket is custom made based on the user's anatomy and the prosthetist's expertise. In our approach, the prosthetist identifies optimal sensor placement, adjusts the socket size to ensure the best fit, and records pressure readings during double-support standing to establish control thresholds. Future investigations could refine this process by focusing on the automated determination of the optimal number, placement, and pressure thresholds of the sensors. By analyzing the pressure distribution across the entire socket–residual limb interface and applying techniques such as local redundancy reduction,[45] the minimum number and ideal sensor positions for effective system control could be identified for each patient, enhancing reliability and adaptability.

Regarding the mechanical strength and durability of the proposed design, it is important to note that there is no universally accepted standard for testing the performance of prosthetic sockets, a subject of ongoing debate within the scientific community.[46–48] While some studies reference ISO 10 328, which outlines static and dynamic fatigue tests for lower-limb prostheses, this standard does not fully address the unique

requirements of prosthetic sockets. In this work, we referred to experimental setups reported in the literature and conducted both static and dynamic tests with axial loads up to 900 N, simulating the single-limb stance and walking conditions of a person weighing 90 kg. These tests demonstrated the socket's structural integrity, showing no signs of damage or cracks. The same tests were conducted with the socket inclined at 10° to evaluate its ability to handle nonaxial forces, further confirming its robustness. Additionally, the cable, constructed from high-strength stainless steel, exhibited no damage or degradation during these tests, confirming its reliability. To further enhance safety and functionality, future work will also investigate alternative cables with higher mechanical strength and flexibility, such as those made from high-performance synthetic fibers. Furthermore, future iterations will include more sophisticated setups, such as those described in Doyen et al.[49] to comprehensively validate the system's mechanical strength and durability and ensure compliance with all safety requirements.

Another limitation of the current system is the weight and size of the control unit, which makes it impossible to integrate directly with the socket, resulting in a less compact and bulkier system. Based on the results obtained in this study, the maximum force required by the system is ≈250 N. Considering the motor and the transmission system currently used, the factor of safety (FOS) is 271 (see "Actuation Unit" for additional details). In the worst-case scenario, where the system needs to support the user's entire weight (assuming a person weighing 90 kg), the FOS would be 75.37. This indicates a high safety margin, suggesting the feasibility of using a more compact motor and transmission system. In future system modifications, an optimized motor and transmission system selection will be performed based on these calculations to ensure an adequate FOS while reducing the weight and bulk of the control unit. The ultimate goal is to integrate the control unit within the prosthetic limb itself, improving system compactness and usability.

4. Experimental Section

Custom Prosthetic Attachment: Design and Simulations: To design the gear teeth of the movable flanges for the custom prosthetic attachment, calculations were performed to verify the main dimensions. These calculations were conducted using Ti–6Al–4 V, which offers optimal performance in terms of weight and mechanical strength and is the suggested material for future developments of the prototype presented in this article, which was made in 316 stainless steel for practical feasibility.

According to Lewis's formula, the tooth can be approximated as a simply supported beam, allowing the calculation of bending stress (σ_b). Then, Hertz's formula can be used to evaluate the contact pressure (P_c).

$$\text{Lewis}: \sigma_b = \frac{F_t}{d\,m\,Y} \approx 216\,\text{MPa} \tag{5}$$

$$\text{Hertz}: P_c = \frac{4F_t}{\pi\,d\,B} \approx 822\,\text{MPa where } B = \sqrt{\frac{8\,F_t}{\pi\,w}\frac{\frac{1-\nu_1^2}{E_1} + \frac{1-\nu_2^2}{E_2}}{\frac{1}{D_1} + \frac{1}{D_2}}} \tag{6}$$

Using the values reported in **Table 1**, the Von Mises stress was calculated to be ≈492 MPa, which was well below the yield point of Ti–6Al4V material, around 850 MPa. One of the disadvantages of using Ti–6Al4V could be its relatively low hardness, which could lead to poor wear and abrasion resistance.[50,51] This could be critical in the dynamic contacts between the pin, flanges, and gears. Therefore, an appropriate treatment

should be carried out in the future for the final prototype in Ti–6Al4V. Various processes can address this issue, including nitriding, ball burnishing, and thermal oxidation.[52–54]

When the design of the prosthetic attachment was completed, its strength was tested by finite-element analyses (FEA) in SolidWorks to verify static stress and fatigue life. Specifically, the custom prosthetic attachment was subjected to the loads identified by Lee et al.[55] during common activities of daily living. To ensure the loads were representative of the most demanding physical activities, the mean loads plus three standard deviations were considered (**Table 2**). The directions of these loads were also reversed and rotated by 90° in the transverse plane to ensure that no premature failure would occur.

The analyses of the entire mechanism and the geared connection were split into two parts to simplify the simulation, and the results are summarized in **Table 3**. Specifically, the prosthetic attachment was able to withstand all applied loads.

Finally, the fatigue life of the mechanism was assessed. Fatigue data of Ti–6Al4V material reported in Janeček et al.[56] were used for the fatigue analysis in SolidWorks. Results showed that the stress levels in the material were too low for the study to converge. This implies that the applied loads were not enough to cause significant stress or failure within the set number of cycles (i.e., 2×10^6 cycles). Therefore, the mechanism can ensure a fatigue life significantly greater than this value under the specified loading conditions.

Table 1. Parameters used in the design of the gear tooth of the flanges of the custom prosthetic attachment.

F_t: tangential force on the gear = 1350 N

d: width of the gear = 19.5 mm

m: module of the gear, i.e., the ratio of the pitch diameter to the number of teeth = 2

Y: Lewis form factor = 0.32

ν: Poisson's ratio = $\nu_1 = \nu_2 = 0.325$[59]

E: Young's modulus = $E_1 = E_2 = 112$ GPa[59,60]

D: diameter = $D_1 = D_2 = 13.7$ mm

Table 2. Loads applied in FEA simulations to assess the static stress on the custom prosthetic attachment.

Position	Value
Proximal	14 Nm
Distal	1282 N
Posterior	54 Nm
Anterior	431 N
Lateral	210 N
Medial	90 Nm

Table 3. Maximum stress result for the different load cases in FEA simulations to assess the static stress on the custom prosthetic attachment when loads reported in Table 2 are applied. FoS: factor of safety. Yield strength of the Ti–6Al4V material equal to 850 MPa.

Load	Stress Full Body [MPa]	FoS	Gear Stress [MPa]	FoS
Literature data	234.0	3.5	218.8	3.5
Reversed	209.6	4	218.8	3.5
Rotated by 90°	272.1	3	364.6	2

Rigid Socket: Design Selection of the Metal Bars: Two metal bars were integrated into the rigid socket during lamination to facilitate the mechanical coupling with the movable flanges of the custom prosthetic attachment. Thus, three samples of metal bars with four different designs were integrated into carbon fiber-reinforced resin structures to test the strength of the bonding interface between the two materials. The designs included plain, bolted (with radius of holes of 3 mm), triangular, and perforated (with radius of holes of 1 mm) metal bars (3 mm thick, 4 cm × 6 cm, aluminum) (**Figure 10**). Specifically, these designs were selected to assess whether a gradual transition between the two materials, which have dissimilar stiffness, could reduce stress concentrations at the interface, as suggested in the state of the art.[57,58] Three samples for each design were subjected to tensile tests until failure, and the results are reported in Figure 10. Contrary to expectation, the plain design exhibited the highest strength. This could be because the holes filled with pure resin acted as weak points, leading to crack initiation or failure under mechanical stress. Another potential reason is that the holes in the perforated design were too small to provide significant benefits, while in the bolted design, the holes were too large, allowing excessive resin flow and reducing the overall bond integrity.

Suspension Performance of the Adjustable Socket System: The suspension performance of the proposed socket system was tested following protocols reported in the state of the art.[34–36] Specifically, a mock residual limb made of fiberglass cast (replicating the shape of the residual limb
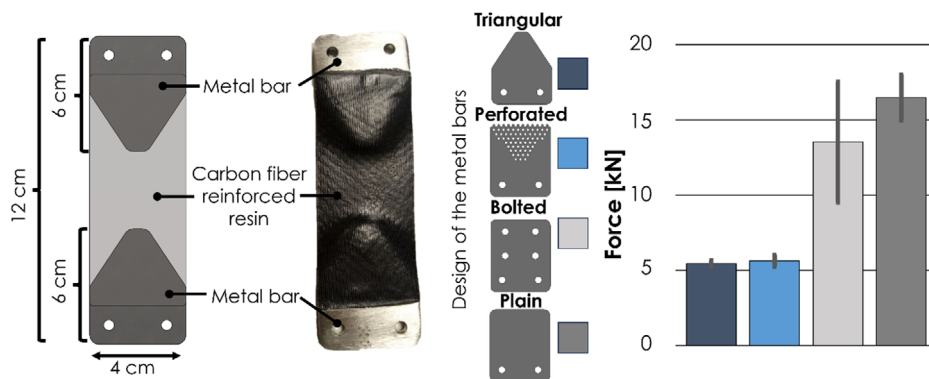

Figure 10. Design of samples used to characterize the strength of the bonding between carbon fiber-reinforced resin and aluminum materials. Various designs of the metal bars were tested to determine if a gradual transition between the two dissimilar materials could reduce stress concentrations at the interface. From top to bottom: triangular, perforated (hole radius: 1 mm), bolted (hole radius: 3 mm), and plain design. The comparison of bonding strength across the different designs indicated the highest strength for the plain design.
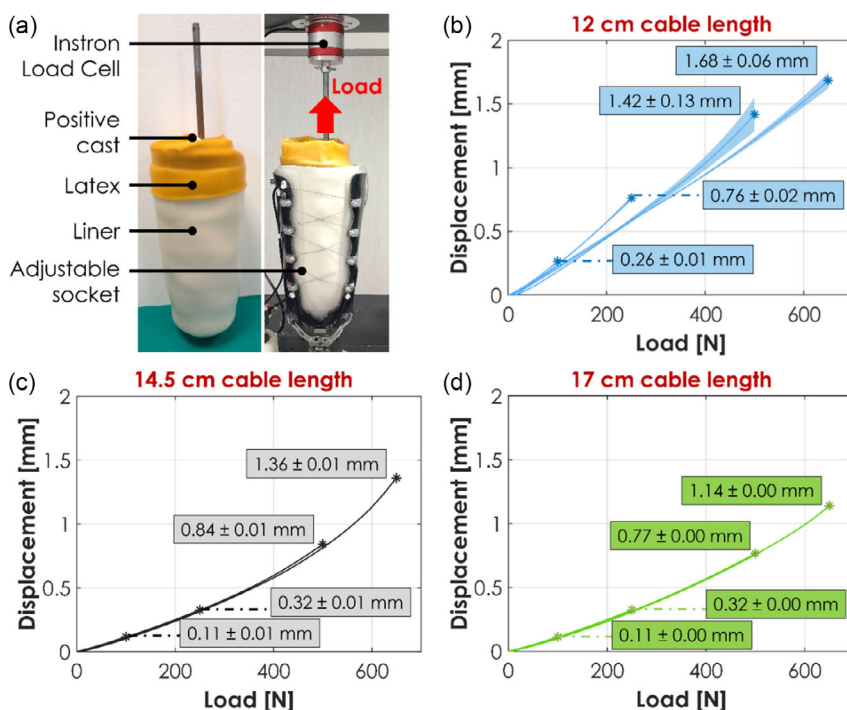

Figure 11. a) Experimental setup and b–d) results of suspension tests on the adjustable socket system. Tests were conducted by pulling a fiberglass cast residual limb mock from 0 to 100 N, 0 to 250 N, 0 to 500 N, and 0 to 650 N at three different cable adjustments of the mechanism: (b) 12 cm (tight), (b) 14.5 cm (very tight), and (c) 17 cm (extremely tight). Ten cycles were performed for each test condition.

simulator) was fabricated, integrating a stainless steel rod for connection with the load cell of an Instron Testing Machine (**Figure 11**). To mimic the effect of skin, a 1 mm-thick latex liner was rolled onto the positive cast. The silicone liner of the socket system was then rolled over the latex layer, placed within the flexible and rigid sockets, and secured at the prosthetic
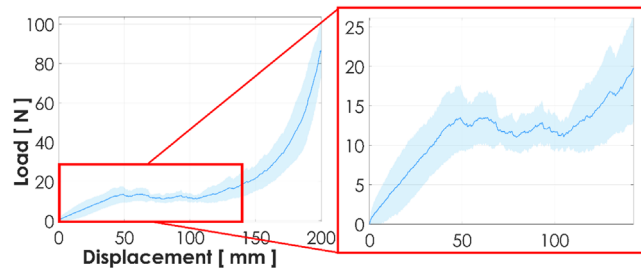

Figure 12. Results of tests conducted using the Instron Testing Machine, where the socket cable was pulled with the socket empty, to evaluate the friction of the cable-driven mechanism.

attachment. The prosthetic attachment was fixed at the base of the Instron Testing Machine, and tensile loads were applied. Tests were conducted with loads ranging from 0 to 100, 0 to 250, 0 to 500, and 0 to 650 N, measuring the pistoning effect, which is defined as the vertical relative displacement of the residual limb (here the mock) with respect to the outer socket and represents a measure of the system's suspension performance.[1] This process was repeated at different lengths of the cable mechanism. Starting from the resting position, the cable mechanism was shortened by 12, 14.5, and 17 cm. Ten cycles for each test condition were carried out.

It should be noted that pressure values were not acquired during these tests because the mock residual limb was made of fiberglass cast. As a result, the pressures at the interface would not be relevant for assessing potential pressures on the residual limb. At the same time, the in vitro simulator was not used, as it would not have supported the loads under analysis.

At 100 N load (Figure 11), the relative displacement between the socket and the mock residual limb was measured to be 0.26 ± 0.01, 0.11 ± 0.01, and 0.11 ± 0.01 mm for 12, 14.5, and 17 cm cable length shortening, respectively. Based on these results, the smart socket passed the suspension test at all three retracted lengths of the cable. Indeed, the relative
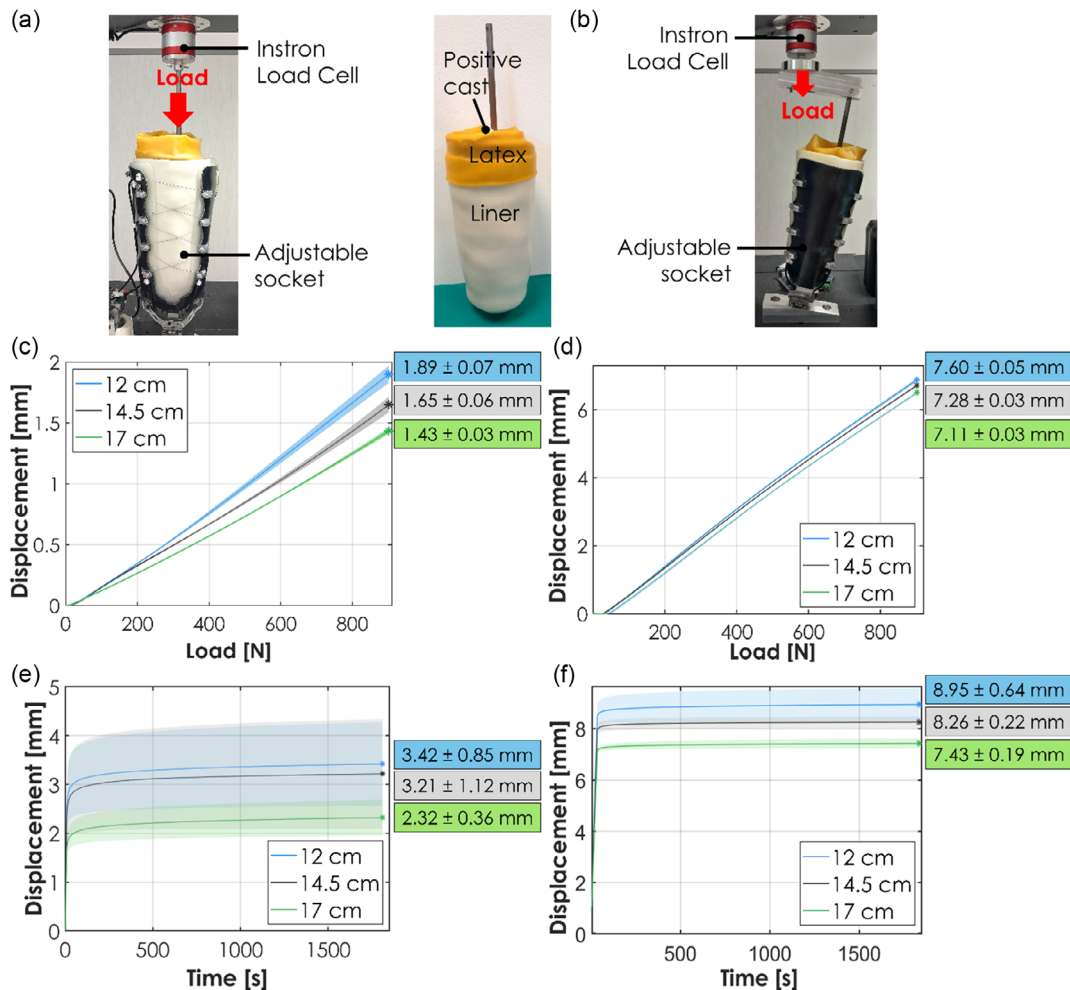

Figure 13. Experimental setup of mechanical strength tests on the adjustable socket system under a) axial and b) nonaxial (10° inclined) loads. Tests were conducted by pushing a fiberglass cast residual limb mock, at three different cable adjustments of the mechanism: 12.5 cm (tight), 14.5 cm (very tight), and 17 cm (extremely tight). Results of dynamic tests with c) axial and d) nonaxial loads: 10 cycles of loading from 0 to 900 N. Results of static tests with e) axial f) nonaxial loads: 900 N load was applied on the socket for 30 min three times.

ADVANCED
SCIENCE NEWS

www.advancedsciencenews.com

ADVANCED
INTELLIGENT
SYSTEMS
Open Access

www.advintellsyst.com

displacement at a tensile load of 100 N was of paramount importance for suspension of a prosthetic socket as it was the range of the load which was experienced by the user during daily life activities and a 10 mm displacement was a well-established failure criterion for suspension.[40] At 650 N load, the relative displacement was 1.68 ± 0.06, 1.36 ± 0.01, and 1.14 ± 0.01 mm for 12, 14.5, and 17 cm cable length shortening, respectively, all successfully meeting the test criteria.

Mechanical Performance of the Adjustable Socket System: The cable used in the adjustable socket system (AISI 316, 7×7 strand, minimum breaking load of 910 N) provides an excellent balance between flexibility and strength and is coated with fluorinated ethylene propylene to minimize friction. Additionally, the cable passes through pulleys designed to further reduce the friction of the system, ensuring smooth operation.

To provide a more quantitative assessment of the friction affecting the system, tests were conducted where the socket cable was pulled using an Instron Testing Machine three consecutive times without any load inside. The results indicated a very low initial pulling force (<20 N), which can be attributed to the friction within the system (**Figure 12**). Subsequently, a significant increase in the pulling force was observed due to the bending stiffness of the lateral and medial parts of the socket.

Subsequently, the mechanical strength of the proposed socket system was tested using the same experimental setup as the suspension tests, but with compressive loads applied under both static and dynamic conditions (**Figure 13**). Specifically, three static tests were performed by applying a 900 N load for 10 min, while dynamic tests involved 10 cycles of loading ranging from 0 to 900 N. This load mimicked the single-limb stance load applied by a user with a body weight of $\approx$90 kg. Additionally, to evaluate the mechanical strength of the socket under nonaxial forces, the same tests were conducted with the socket inclined at 10°. All tests were conducted at the three different lengths of the cable mechanism (12, 14.5, and 17 cm).

After tests (Figure 13), the smart socket did not show any signs of damage or cracks in any of the structural components of the socket. At 900 N compression axial load (Figure 13c,e), the relative displacement between the socket system and the mock residual limb was measured to be 1.89 ± 0.07, 1.65 ± 0.06, and 1.43 ± 0.03 mm, in dynamic tests, and 3.42 ± 0.85, 3.21 ± 1.12, and 2.32 ± 0.36 mm, in static tests, for 12, 14.5, and 17 cm cable length shortening, respectively. At 900 N compression nonaxial load (Figure 13d,f), the relative displacement between the socket system and the mock residual limb was measured to be 7.60 ± 0.05, 7.28 ± 0.03, and 7.11 ± 0.03 mm, in dynamic tests, and 8.95 ± 0.64, 8.26 ± 0.22, and 7.43 ± 0.19 mm, in static tests, for 12, 14.5, and 17 cm cable length shortening, respectively. These displacements were likely caused by the compression of the silicone liner at the distal end.

Sensorized Liner: FSR Sensors Calibration: The FSR sensors embedded into the liner were calibrated using an Instron Testing Machine to ensure accurate pressure measurement. The calibration process involved performing three cycles, where pressure was incrementally applied from 0 kPa up to 140 kPa, simulating the typical range of interface pressure in transfemoral sockets.[11] During each cycle, the output voltage generated by the sensors was recorded. Subsequently, a reverse calibration curve was computed for each sensor individually, which involved mapping the sensor output back to the corresponding pressure values (**Figure 14**). The final values for hysteresis and linearity are reported in **Table 4** for each sensor.

Transfemoral Residual Limb Simulator: Manufacturing: For the manufacturing of the residual limb simulator different silicones were used to mimic the mechanical properties of different biological tissues. Specifically, silicone Dragon Skin 20 (Shore Hardness: 20 A, Smooth-on Inc.), colored with pink Silc Pig, was poured into specific molds for the manufacturing of rectus femoris, biceps femoris, vastus lateralis, and vastus medialis muscles. The muscles were fixed in place on the hip anatomical model using Sil-Poxy silicone glue and positioned within the negative cast of a transfemoral residual limb. The negative cast internal surface was coated with a 5 mm-thick plastic layer and then filled with silicone Ecoflex 0010 (Shore Hardness: 00-10, Smooth-on Inc.) to simulate fat tissues. Afterward, the plastic layer was removed, and the external fat surface was covered with a 1 mm-thick plastic layer. The empty space was filled with Dragon Skin 10 (Shore Hardness: 10 A, Smooth-on Inc.) to
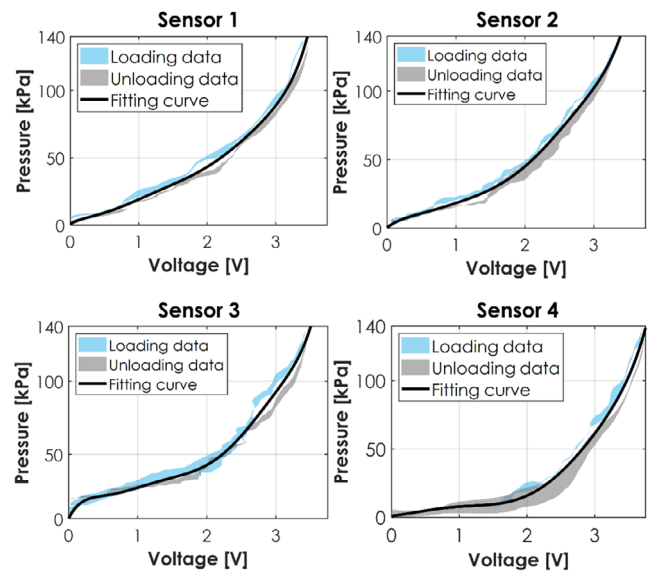

Figure 14. Reverse calibration curves of the FSR sensors embedded in the prosthetic liner.

Table 4. Hysteresis and linearity values for each FSR sensor.

	Hysteresis [kPa]	Linearity [kPa]
Sensor 1	3.46	31.65
Sensor 2	2.97	21.19
Sensor 3	3.38	65.33
Sensor 4	6.04	15.20

mimic skin. Upon pouring, the plastic layer was removed, creating an empty chamber for the hydraulic actuation that was sealed using Sil-Poxy silicone glue. Finally, two fluidic tubes were integrated and used for the connection with the two syringe pumps.

Actuation Unit: The control unit of the smart socket system featured a DC motor capable of delivering a maximum torque of 0.7 Nm and paired with a planetary gearbox that had a 43:1 reduction ratio. The gearbox's output shaft was connected to a worm gear assembly, consisting of a single-thread worm and a 50-tooth worm wheel. The worm wheel had a diameter of 50 mm and included a cylindrical protrusion with a 30 mm diameter ($r_0 = 15$ mm), around which the cable was wound. Based on the results described above, the maximum force was measured to be 238.03 ± 3.60 N at initial volume of the simulator and 24 cm cable shortening (Figure 7). Thus, the operating range of the system should not require a tension exceeding 250 N or a cable shortening of more than 24 cm. Considering these requirements, it was essential to evaluate the transmission system connecting the motor to the cable winding drum (i.e., cylindrical protrusion of the worm wheel) and the formula that correlates the motor torque (τ) and cable tension (T) (**Figure 15**).

$$T = \frac{\tau}{r_0 + \frac{t}{\pi}\theta} \qquad (7)$$

where θ is the angular displacement of the motor and t the cable thickness (i.e., 1.2 mm). The formula took into account the effective radius of the drum after a given angular displacement, as the cable wound around it. Consequently, the effective radius of the drum ($r_0 = 15$ mm) increased with each complete turn (n). Additionally, the length of cable wound was given by the formula
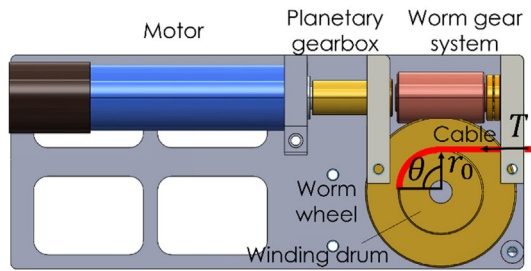
Figure 15. Design overview of the actuation system in the control unit, which includes a DC motor coupled with a planetary gearbox and a worm gear system. The worm gear system consists of a single-thread worm and a worm wheel with a cylindrical protrusion around which the cable is wound.

$$L_{turn} = 2\pi \left(r_0 + 2nt\right) \tag{8}$$

Thus, the total length of cable wound after 3 turns was 32.78 cm, largely covering the required range. After 3 turns, the torque at the system's output needed to generate a tension of 250 N was 5.55 Nm. Since the transmission system included a planetary gearbox with a reduction ratio of 43:1 and a worm gear system with a reduction ratio of 50:1, the torque required at the motor was 2.58 mNm. Considering that the Faulhaber motor can provide a maximum torque of 0.7 Nm, the FOS, that is., the ratio between the maximum capacity of the system and the demanded load, turned out to be 271. Considering the worst-case scenario in which the system must support a maximum load of 900 N, equivalent to the weight of a person of 90 kg, the FOS would be 75.37. This indicates a very high margin of safety, demonstrating that the system is more than capable of handling the load effectively. In future modifications of the system, an optimized selection will be made based on these calculations to ensure an adequate FOS while reducing the weight and bulk of the control unit, with the goal of integrating it within the limb prosthesis.

Supporting Information

Supporting Information is available from the Wiley Online Library or from the author.

Conflict of Interest

The authors declare no conflict of interest.

Author Contributions

Linda Paternò: conceptualization (lead); data curation (equal); formal analysis (lead); funding acquisition (supporting); investigation (lead); methodology (lead); supervision (lead); validation (equal); writing—original draft (lead); writing—review & editing (lead). **Ahmed Zohaib Zaidi**: conceptualization (supporting); data curation (equal); formal analysis (equal); investigation (equal); methodology (equal); validation (equal); writing—original draft (supporting); writing—review & editing (supporting). **Maria Grazia Polizzotto**: data curation (supporting); formal analysis (supporting); investigation (supporting); methodology (supporting); validation (supporting); writing—original draft (supporting); writing—review & editing (supporting). **Sofia Dalmiani**: conceptualization (supporting); investigation (supporting); methodology (supporting); validation (supporting); writing—review & editing (supporting). **Djoeke Helsloot**: data curation (supporting); formal analysis (supporting); investigation (supporting); methodology (supporting); validation (supporting); writing—review & editing (supporting). **Sybren Heikens**: conceptualization (supporting); data curation (supporting); formal analysis (supporting); investigation (supporting); methodology (supporting); writing—review & editing (supporting). **Emanuele Gruppioni**: conceptualization (supporting); funding acquisition (equal); project administration (equal); supervision (supporting); writing—review & editing (supporting). **Arianna Menciassi**: conceptualization (supporting); formal analysis (supporting); funding acquisition (lead); methodology (supporting); project administration (lead); resources (lead); supervision (lead); writing—original draft (supporting); writing—review & editing (lead).

Data Availability Statement

The data that support the findings of this study are available from the corresponding author upon reasonable request.

[1] L. Paternò, M. Ibrahimi, E. Gruppioni, A. Menciassi, L. Ricotti, *IEEE Trans. Biomed. Eng.* **2018**, *65*, 1996.

[2] R. Gailey, K. Allen, J. Castles, J. Kucharik, M. Roeder, *J. Rehabil. Res. Dev.* **2008**, *45*, 15.

[3] R. Safari, *Prosthet. Orthot. Int.* **2020**, *44*, 384.

[4] J. Seo, H. Lee, D. W. Seo, D. Lee, O. Kwon, M. K. Kwak, K. H. Lee, *Sensors* **2021**, *21*, 407.

[5] S. Turner, A. H. McGregor, *Arch. Rehabil. Res. Clin. Transl.* **2020**, *2*, 100059.

[6] R. Bekrater-Bodmann, *Front. Neurorob.* **2021**, *14*, 604376.

[7] E. C. Baars, E. Schrier, P. U. DIjkstra, J. H. B. Geertzen, *Medicine* **2018**, *97*, e12296.

[8] S. Manz, R. Valette, F. Damonte, L. Avanci Gaudio, J. Gonzalez-Vargas, M. Sartori, S. Dosen, J. Rietman, *J. NeuroEng. Rehabil.* **2022**, *19*, 1.

[9] J. E. Sanders, S. Fatone, *J. Rehabil. Res. Dev.* **2011**, *48*, 949.

[10] L. Paternò, M. Ibrahimi, E. Rosini, G. Menfi, V. Monaco, E. Gruppioni, L. Ricotti, A. Menciassi, *Sci. Rep.* **2021**, *11*, 12273.

[11] L. Paternò, L. Truppa, M. Ibrahimi, E. Rosini, E. Gruppioni, L. Ricotti, A. Menciassi, *Prosthet. Orthot. Int.* **2023**, *48*, 176.

[12] M. Baldock, N. Pickard, M. Prince, S. Kirkwood, A. Chadwell, D. Howard, A. Dickinson, L. Kenney, N. Gill, S. Curtin, *J. Neuroeng. Rehabil.* **2023**, *20*, 1.

[13] Prosthetics and Orthotics Solutions | Adjustable Prosthetic Socket | BOA System | Prosthesis Doctor | Adaptive Athlete | Amputee Information | O&P Solution | Click Medical.

[14] Varos socket | Ottobock.

[15] ConnectTF Adjustable Socket for Low Active TF Amputees, Ossur. com (accessed: November 2024).

[16] Quorum Prosthetics.

[17] Infinite Socket TF | LIM Innovations.

[18] Above Knee Socket-less SocketTM — Martin Bionics, https:// martinbionics.com/ (accessed: November 2024).

[19] iFIT Prosthetics - Home.

[20] G. Pirouzi, N. A. Abu Osman, A. A. Oshkour, S. Ali, H. Gholizadeh, W. A. B. Wan Abas, *Sensors* **2014**, *14*, 16754.

[21] K. H. Lee, H. S. Heo, J. Kim, J. H. Cho, K. T. Kim, J. Y. Hur, J. H. Kim, Y. Lee, *Sensors* **2023**, *24*, 133.

[22] E. J. Weathersby, J. L. Garbini, B. G. Larsen, J. B. McLean, A. C. Vamos, J. E. Sanders, *IEEE Trans. Biomed. Eng.* **2021**, *68*, 36.

[23] E. J. Weathersby, A. C. Vamos, B. G. Larsen, J. B. McLean, R. V. Carter, K. J. Allyn, D. Ballesteros, H. Wang, N. S. deGrasse, J. L. Friedly, B. J. Hafner, J. L. Garbini, M. A. Ciol, J. E. Sanders, *J. Rehabil. Assistive Technol. Eng.* **2022**, *9*, 205566832210932.

[24] H. Choi, B. B. Kang, B. K. Jung, K. J. Cho, *IEEE Rob. Autom. Lett.* **2019**, *4*, 4499.

[25] L. Paterno, M. Filosa, E. Anselmino, E. Gruppioni, I. C. Protesi, A. Mazzoni, S. Micera, A. Menciassi, *Soft Transfemoral Prosthetic Socket with EMG Sensing and Augmenting Feedback: A Case Study*, IEEE Transactions on Medical Robotics and Bionics **2023**.

[26] H. Gholizadeh, N. A. A. Osman, A. Eshraghi, N. A. Abd Razak, *Biomed. Eng. Online* **2014**, *13*, 1.

[27] M. S. Jamaludin, A. Hanafusa, Y. Shinichirou, Y. Agarie, H. Otsuka, K. Ohnishi, *Bioengineering* **2019**, *6*, 98.

[28] S. T. Ko, F. Asplund, B. Zeybek, *Sensors* **2021**, *21*, 5016.

[29] V. Sanchez, C. J. Walsh, R. J. Wood, V. Sanchez, C. J. Walsh, A. Wood John, R. J. Paulson, R. J. Wood, *Adv. Funct. Mater.* **2021**, *31*, 2008278.

[30] L. Paternò, L. Lorenzon, *Front. Rob. AI* **2023**, *10*, 1075634.

[31] Z. Duanmu, S. J. V. Ali, J. Allen, L. K. Cheng, M. Stommel, W. Xu, *IEEE Trans. Biomed. Eng.* **2024**, *71*, 2042.

[32] M. Cianchetti, C. Laschi, A. Menciassi, P. Dario, *Nat. Rev. Mater.* **2018**, *3*, 143.

[33] J. L. Sparks, N. A. Vavalle, K. E. Kasting, B. Long, M. L. Tanaka, P. A. Sanger, K. Schnell, T. A. Conner-Kerr, *Adv. Skin Wound Care* **2015**, *28*, 59.

[34] J. Quinlan, J. Yohay, V. Subramanian, B. Poziembo, S. Fatone, *PLoS One* **2020**, *15*, e0237841.

[35] S. Kim, S. V. Yalla, S. Shetty, N. J. Rosenblatt, *Results Mater.* **2024**, *21*, 100549.

[36] F. Gariboldi, M. Scapinello, N. Petrone, G. L. Migliore, G. Teti, A. G. Cutti, *Med. Eng. Phys.* **2023**, *114*, 103970.

[37] F. Jasni, N. A. Hamzaid, A. G. A. Muthalif, Z. Zakaria, H. N. Shasmin, S. C. Ng, *IEEE/ASME Trans. Mechatron.* **2016**, *21*, 2466.

[38] J. Tabor, T. Agcayazi, A. Fleming, B. Thompson, A. Kapoor, M. Liu, M. Y. Lee, H. Huang, A. Bozkurt, T. K. Ghosh, *IEEE Sens. J.* **2021**, *21*, 9413.

[39] E. A. Al-Fakih, N. A. Abu Osman, F. R. Mahamd Adikan, A. Eshraghi, P. Jahanshahi, *IEEE Sens. J.* **2016**, *16*, 965.

[40] Z. F. Zhang, X. M. Tao, H. P. Zhang, B. Zhu, *IEEE Sens. J.* **2013**, *13*, 1478.

[41] E. A. Al-Fakih, N. A. Abu Osman, F. R. Mahmad Adikan, *Sensors* **2016**, *16*, 1119.

[42] S. T. Ko, F. Asplund, B. Zeybek, *Sensors* **2021**, *21*, 5016.

[43] M. Hopkins, R. Vaidyanathan, A. H. McGregor, *IEEE Sens. J.* **2020**, *20*, 6992.

[44] G. Pirouzi, N. A. Abu Osman, A. Eshraghi, S. Ali, H. Gholizadeh, W. A. B. Wan Abas, *Sci. World J.* **2014**, *2014*, 849073.

[45] S. Mukhopadhyay, N. Cennamo, M. J. Deen, J. Lee, S. Morais, W. Zhu, Y. Chen, S.-T. Ko, Z. Lu, *Sensors* **2022**, *22*, 3103.

[46] F. Gariboldi, D. Pasquarelli, A. G. Cutti, *Med. Eng. Phys.* **2022**, *99*, 103742.

[47] A. Dickinson, E. Nickel, S. Fatone, F. Gariboldi, J. Steer, A. G. Cutti, J. Erenstone, S. Zahedi, *Prosthet. Orthot. Int.* **2023**, *47*, 1.

[48] F. Gariboldi, A. G. Cutti, S. Fatone, E. Nickel, A. Dickinson, J. Steer, J. Erenstone, S. Zahedi, *Prosthet. Orthot. Int.* **2023**, *47*, 3.

[49] É. Doyen, F. Szmytka, J. F. Semblat, *Sci. Rep.* **2023**, *3*, 5226.

[50] C. Ohkubo, I. Shimura, T. Aoki, S. Hanatani, T. Hosoi, M. Hattori, Y. Oda, T. Okabe, *Biomaterials* **2003**, *24*, 3377.

[51] X. Liu, P. K. Chu, C. Ding, *Mater. Sci. Eng.: R: Rep.* **2004**, *47*, 49.

[52] G. D. Revankar, R. Shetty, S. S. Rao, V. N. Gaitonde, *J. Mater. Res. Technol.* **2017**, *6*, 13.

[53] A. Bloyce, P. Y. Qi, H. Dong, T. Bell, *Surf. Coat. Technol.* **1998**, *107*, 125.

[54] J. R. Deepak, *Appl. Mech. Mater.* **2015**, *766*, 618.

[55] W. C. C. Lee, L. A. Frossard, K. Hagberg, E. Haggstrom, R. Brånemark, J. H. Evans, M. J. Pearcy, *Clin. Biomech.* **2007**, *22*, 665.

[56] M. Janeček, F. Nový, P. Harcuba, J. Stráský, L. Trško, M. Mhaede, L. Wagner, *Acta Phys. Pol. A* **2015**, *4*, 497.

[57] A. Pramanik, A. K. Basak, Y. Dong, P. K. Sarker, M. S. Uddin, G. Littlefair, A. R. Dixit, S. Chattopadhyaya, *Composites, Part A* **2017**, *101*, 1.

[58] E. I. Avgoulas, M. P. F. Sutcliffe, *Compos. Struct.* **2016**, *152*, 929.

[59] M. Kikuchi, M. Takahashi, O. Okuno, *Dent. Mater.* **2006**, *22*, 641.

[60] M. Niinomi, *Mater. Sci. Eng., A* **1998**, *243*, 231.